



**Collective dynamics in liquid aluminium oxide: *Ab initio* analysis of collective eigenmodes**Maria Kopcha <sup>1</sup>, Taras Bryk <sup>1,2</sup>, Jean-François Wax,<sup>3</sup> and Noël Jakse <sup>4</sup><sup>1</sup>*Institute for Condensed Matter Physics of the National Academy of Sciences of Ukraine, 1 Svientsitskii Street, UA-79011 Lviv, Ukraine*<sup>2</sup>*Lviv Polytechnic National University, UA-79013 Lviv, Ukraine*<sup>3</sup>*Laboratoire de Chimie et de Physique A2MC, Université de Lorraine, Metz, 1, Boulevard Arago 57078 Metz Cedex 3, France*<sup>4</sup>*Université Grenoble Alpes, CNRS, Grenoble INP, SIMaP, F-38000 Grenoble, France*

(Received 19 July 2023; accepted 27 November 2023; published 15 December 2023)

Collective dynamics in molten alumina is studied by a combination of *ab initio* molecular dynamics (AIMD) simulations and theoretical analysis of time correlation functions. Two models of dynamics in molten salts are used to analyze time correlation functions: a six-variable viscoelastic model and an eight-variable thermoviscoelastic one. The corresponding sets of dynamic variables are used to construct  $6 \times 6$  and  $8 \times 8$  generalized hydrodynamic matrices, eigenmodes of which represent (wave number)  $k$ -dependent propagating and relaxing processes. It is shown that the thermoviscoelastic model is able to recover the AIMD-derived partial current-current time correlation functions, represented *via* contributions of the eight  $k$ -dependent collective eigenmodes. Dispersion and damping of three branches of propagating eigenmodes are compared to the numerical estimates from peak positions of corresponding current spectral functions in order to rationalize effects of acoustic, longitudinal and transverse opticlike excitations in collective dynamics of molten alumina. The role of another branch of propagating eigenmodes in recovering the frequencies and damping of long-wavelength longitudinal optic-like modes estimated from AIMD-derived spectral current functions is discussed.

DOI: [10.1103/PhysRevB.108.224204](https://doi.org/10.1103/PhysRevB.108.224204)**I. INTRODUCTION**

Microscopic structure and dynamics of solid and liquid oxides, as well as of their nanoparticles, is of great interest due to numerous applications of the oxides' nanotechnology and electrochemistry [1–3]. In particular, alumina,  $\text{Al}_2\text{O}_3$ , nanoparticles are one of the most extensively used nanometallic oxides and nanofillers due to their fascinating properties in everyday applications. Aluminium oxide is an ionic compound and is used in aluminium production, when electrolysis of the alumina/cryolite solution gives aluminium at the cathode and oxygen at the anode. Moreover, the aluminum oxide was found in significant amounts in brain specimens of patients with Alzheimer's disease [4,5], which has caused a discussion about the effect of aluminium pots and dishes in the development of Alzheimer's disease. From a scientific point of view, molten oxides such as  $\text{Al}_2\text{O}_3$  represent an additional challenge for understanding their transport properties and collective dynamics. As a matter of fact, these oxides are characterized not only by polarizability effects but also by partial charges, covalent oxygen bonding, and triply bonded oxygen, leading to the appearance of  $\text{AlO}_5$  structural units that impact the shear viscosity and collective dynamics [6].

Experimental studies of collective dynamics of  $\text{Al}_2\text{O}_3$  were limited mainly to inelastic x-ray scattering (IXS) for liquid and supercooled states in a range of temperatures from 2300 to 3100 K [7], the melting point being  $T_m = 2327$  K [8]. More recently, the structure factor was measured from x-ray diffraction experiments [9]. Given the scarcity of the measurements, atomic-scale simulations such as molecular dynamics provide a powerful and complementary means for a deeper understanding of the dynamics.

The atomistic structure and dynamics of alumina melts were studied by computer simulations [9–16] using different interaction models. Three potential models were derived from density functional theory (DFT) using the local-density approximation (LDA), the generalized gradient approximation (GGA), and the meta-GGA functional within the strongly constrained and appropriately normed (SCAN) functional approach [17] respectively. Jahn *et al.* [12] developed a fully flexible ionic interaction model for alumina accounting for ionic polarizability and shape deformations up to the quadrupolar level and derived two versions based respectively on the LDA and the GGA. On this basis, the sound velocity of about  $v_s = 7350$  m/s at  $T = 2350$  K was further reported [13], and the vibrational density of states and the dispersion of acoustic modes were studied [14]. The dispersion relations and line widths were obtained from the maxima of the partial longitudinal current correlation spectra and from fits of the total x-ray-weighted dynamic structure factor  $S(k, \omega)$  with a Lorentzian model, with  $k$  and  $\omega$  being the wave number and the frequency, respectively. An estimate for a sound velocity was made as 6800 m/s at  $T = 2500$  K [14]. The SCAN-based potential gives also a very good description of the melt properties such as the local structure and self-diffusion coefficients [16], but was not exploited for the collective dynamics for now.

Theoretical models should recover details of collective dynamics in molten salts and oxides, especially on nanoscales with explicit accounting for atomistic structure (nonhydrodynamic effects). Simple hydrodynamic models for binary ionic liquids address only slow processes stemming from local conservation laws, which are inadequate for typical temporal and spatial scales of processes measured in IXS

experiments or observed in the shape of time correlation functions from molecular dynamics simulations. One of the most promising directions in theoretical modeling of collective dynamics in liquids and ionic melts, in particular, is based on an extension of the hydrodynamic treatment with additional balance equations for nonhydrodynamic dynamic variables. The latter can be performed within a matrix form of the generalized Langevin equation known as the generalized collective modes (GCM) framework [18,19]. For ionic melts, a very specific feature of collective dynamics is in the behavior of charge-density time correlations, which are affected by nonhydrodynamic optic modes, in contrast to the case of simple liquid mixtures [20]. Early attempts to obtain dispersion curves of collective excitations for NaCl and NaI within the parameter-free GCM approach [21] showed a mismatch between theory and experimental results [22,23], possibly due to the neglect of polarization effects. Next *ab initio* GCM studies of dynamics in molten salts were performed with the full accounting for polarization of the electron subsystem, and based on the viscoelastic dynamic model [24,25]. This approach improved the dispersion curves; however, it was unable to recover well the simulation-derived partial density-density and current-current time correlation functions. New IXS experiments for NaI [26] and NaCl [27] revived the interest in the dispersion law of nonhydrodynamic opticlike excitations. Recently, an extended thermoviscoelastic dynamic model was suggested [28] that showed promising results in recovering the correct behavior of time correlation functions in ionic melts.

The aim of this study is to apply the recently suggested eight-variable GCM methodology to analyze time correlation functions of nonsimple ionic melt  $\text{Al}_2\text{O}_3$  and estimate the dispersion of acoustic and nonhydrodynamic optic modes. For this purpose, the time correlation functions were determined from *ab initio* molecular dynamics (AIMD) simulations based on DFT with the SCAN functional to preserve the best accuracy that would probably be less with empirical potentials. The main finding of this study lies in the application of the eight-variable model that allows one to recover AIMD-derived partial current-current time correlation functions with good precision. Furthermore, the eight-variable model is necessary to explain the time dependence of longitudinal current correlations in this oxide melt as in molten salts previously studied [28], pointing towards the generality of this theoretical approach, which can represent a basis for the understanding of collective dynamics in liquids with long-range interactions. The remaining part of the paper is organized as follows. In the Sec. II technical details of AIMD simulations of liquid  $\text{Al}_2\text{O}_3$  are reported and details of the theoretical analysis framework are developed. Section III contains the main results on static structure and on single-particle and collective dynamics and the corresponding discussion. The last section draws the conclusions.

## II. COMPUTATIONAL AND THEORETICAL BACKGROUND

### A. *Ab initio* molecular dynamics simulations

The *ab initio* molecular dynamics simulations were performed within the DFT [29,30] using the Vienna *ab initio*

simulation package [31,32] (VASP) in version 5.4.4. Cubic simulation supercells were set up with periodic boundary conditions and a number of  $N = 300$  atoms, out of which 120 were Al atoms and 180 were O atoms. The projector augmented-wave method with a cutoff energy set to 600 eV (beyond the recommended value for the potentials) was used to describe the electron-ion interactions [33,34]. This larger cutoff guarantees an accurate determination of the pressure. Exchange-correlation effects were taken into account within the meta-GGA functional within the strongly constrained and appropriately normed (SCAN) functional approach [17]. The latter was proven relevant for several oxides in the crystalline and molten states including alumina [16,35,36]. As far as the liquid phase is concerned, and quite a large number of particles was used in simulations, only the  $\Gamma$  point was used in sampling the Brillouin zone. The dynamics were performed within Newton's equations of motion, integrated numerically using the Verlet algorithm in the velocity form with a time step of 1 fs.

The phase-space trajectory was determined in the canonical ensemble, namely, constant numbers of atoms  $N$ , volume  $V$ , and temperature  $T$  ( $NVT$ ), by means of a Nosé thermostat [37,38]. We checked out the temperature fluctuations to make sure they were practically not affected by introduction of the thermostat. We have to mention that the thermostat coupled to the simulated system can bias the dynamics as it was shown in Ref. [39]. Our simulation was conducted at  $T = 2400$  K, and the size of the supercell was adjusted to get a pressure close to zero with a residual value of less than 0.37 GPa, which is lower than the amplitude of pressure fluctuations during the simulation. The resulting equilibrium atomic volume was found to be  $11.60 \text{ \AA}^3$ , close to the experimental value  $11.58 \text{ \AA}^3$  [40]. After pressure adjustment and equilibration, the duration of the runs was 41 ps in order to produce the physical properties. It was shown [16] that the AIMD results are in good agreement with the x-ray diffraction experiments [9] for the total structure factor and are consistent with the tracer diffusion measurements [41] for the self-diffusion coefficient of oxygen.

### B. Generalized collective modes approach

In order to analyze AIMD-derived time correlation functions, the generalized hydrodynamic approach to collective dynamics of binary liquids is used. For a description of the very long-wavelength dynamics in the particular case of oxide melts, it is enough to start from consideration of hydrodynamic fluctuations (fluctuations of conserved quantities) of four dynamic variables:

$$\mathbf{A}^{(\text{hyd})}(k, t) = \{n_t(k, t), n_Q(k, t), J^t(k, t), e(k, t)\}, \quad (1)$$

where  $n_t(k, t)$  and  $n_Q(k, t)$  are the spatial Fourier components of the total number density and the charge density, respectively;  $J^t(k, t)$  is the spatial Fourier component of the total mass-current density; and  $e(k, t)$  is the spatial Fourier component of the energy density. However, outside the hydrodynamic regime (and the wave numbers in AIMD simulations as well as in IXS experiments are outside hydrodynamics), the hydrodynamic description of collective dynamics is not sufficient to explain the dynamic processes and one has to make use of the extended sets of dynamic variables, which enable

treatment of nonhydrodynamic processes [42]. In the actual study a thermoviscoelastic dynamic model of locally coupled (with the same  $k$ ) fluctuations is adopted, which forms a set of  $N_v = 8$  dynamic variables:

$$\mathbf{A}^{(8)}(k, t) = \{n_{\text{Al}}(k, t), n_{\text{O}}(k, t), J_{\text{Al}}^L(k, t), J_{\text{O}}^L(k, t), \\ \times e(k, t), J_{\text{Al}}^L(k, t), J_{\text{O}}^L(k, t), \dot{e}(k, t)\}, \quad (2)$$

where

$$n_{\alpha}(k, t) = \frac{1}{\sqrt{N_{\alpha}}} \sum_{j=1}^{N_{\alpha}} e^{-i\mathbf{k}\mathbf{r}_{j,\alpha}(t)}, \quad \alpha = \text{Al}, \text{O}, \quad (3)$$

are the spatial Fourier components of partial particle densities,

$$J_{\alpha}^{L/T}(k, t) = \frac{m_{\alpha}}{\sqrt{N_{\alpha}}} \sum_{j=1}^{N_{\alpha}} v_{j,\alpha}^{L/T}(t) e^{-i\mathbf{k}\mathbf{r}_{j,\alpha}(t)}, \quad \alpha = \text{Al}, \text{O}, \quad (4)$$

are the spatial Fourier-components of partial mass-current densities;  $m_{\alpha}$  and  $N_{\alpha}$  are the mass and number of atoms of the  $\alpha$  species, respectively;  $\mathbf{k}$  is the wave vector;  $\mathbf{r}_{j,\alpha}(t)$  is the particle position; and  $v_{j,\alpha}^{L/T}(t)$  is the longitudinal or transverse component of the particle velocity, while the summation for each partial variable is performed over the particles of kind  $\alpha$ . The total mass-current in Eq. (1) is simply

$$J_{\text{tot}}^{L/T}(k, t) = \sqrt{c_{\text{Al}}} J_{\text{Al}}^{L/T}(k, t) + \sqrt{c_{\text{O}}} J_{\text{O}}^{L/T}(k, t), \quad (5)$$

with regular concentration of species  $c_{\alpha}$ , and the overdots in Eq. (2) mean the first time derivative of the corresponding variable. A simplified dynamic model, the  $N_v = 6$  variable viscoelastic (ve) one,

$$\mathbf{A}^{(\text{ve})}(k, t) = \{n_{\text{Al}}(k, t), n_{\text{O}}(k, t), J_{\text{Al}}^L(k, t), J_{\text{O}}^L(k, t), \\ \times J_{\text{Al}}^L(k, t), J_{\text{O}}^L(k, t)\}, \quad (6)$$

does not contain contributions from the energy (heat) density or the energy (heat)-current density, which makes possible

simple evaluation of all static and dynamic correlation for GCM analysis directly from AIMD. The chosen set of dynamic variables is used to construct a  $N_v \times N_v$  generalized hydrodynamic matrix  $\mathbf{T}(k)$ , eigenvalues  $z_j(k)$  of which correspond to wave-number-dependent collective modes. Note that for propagating eigenmodes one obtains pairs of complex-conjugated eigenvalues

$$z_j(k) = \sigma_j(k) \pm i\omega_j(k), \quad (7)$$

with the real part  $\sigma_j(k)$  corresponding to the  $k$ -dependent damping, and  $\omega_j(k)$  corresponding to the dispersion of the  $j$ th branch of collective excitations, while purely real eigenvalues [we mark them as  $d_j(k)$ ],

$$z_j(k) \equiv \text{Re}[z_j(k)] = d_j(k), \quad (8)$$

correspond to relaxation processes in the melt. For longitudinal dynamics there must exist in the long-wavelength region at least two relaxation processes:  $d_1(k) \propto k^2$ , related mainly to thermal diffusivity, and  $d_2(k)$ , tending in the long-wavelength limit to a nonzero constant due to the local electroneutrality condition.

Within the GCM approach the  $8 \times 8$  generalized hydrodynamic matrix  $\mathbf{T}(k)$ , obtained on the set of dynamic variables (2), is expressed in the following way [18]:

$$\mathbf{T}(k) = \mathbf{F}(k, t=0) \tilde{\mathbf{F}}^{-1}(k, z=0), \quad (9)$$

via the  $N_v \times N_v$  matrices of static correlation functions  $\mathbf{F}(k, t=0)$  and of Laplace-transformed time correlation functions in the Markovian approximation  $\tilde{\mathbf{F}}(k, z=0)$  [18,43]. For the case of the eight-variable set of dynamic variables (2), one has to calculate for each wave number  $k$  the  $8 \times 8$  matrix of static correlations,

$$\mathbf{F}(k, t=0) = \begin{pmatrix} f_{n_{\text{Al}}n_{\text{Al}}} & f_{n_{\text{Al}}n_{\text{O}}} & 0 & 0 & f_{n_{\text{Al}}e} & -i\frac{k}{m_{\text{Al}}}f_{J_{\text{Al}}J_{\text{Al}}} & 0 & 0 \\ f_{n_{\text{Al}}n_{\text{O}}} & f_{n_{\text{O}}n_{\text{O}}} & 0 & 0 & f_{n_{\text{O}}e} & 0 & -i\frac{k}{m_{\text{O}}}f_{J_{\text{O}}J_{\text{O}}} & 0 \\ 0 & 0 & f_{J_{\text{Al}}J_{\text{Al}}} & 0 & 0 & 0 & 0 & -if_{J_{\text{Al}}e} \\ 0 & 0 & 0 & f_{J_{\text{O}}J_{\text{O}}} & 0 & 0 & 0 & -if_{J_{\text{O}}e} \\ f_{n_{\text{Al}}e} & f_{n_{\text{O}}e} & 0 & 0 & f_{ee} & -if_{J_{\text{Al}}e} & -if_{J_{\text{O}}e} & 0 \\ i\frac{k}{m_{\text{Al}}}f_{J_{\text{Al}}J_{\text{Al}}} & 0 & 0 & 0 & if_{J_{\text{Al}}e} & f_{J_{\text{Al}}J_{\text{Al}}} & f_{J_{\text{Al}}J_{\text{O}}} & 0 \\ 0 & i\frac{k}{m_{\text{O}}}f_{J_{\text{O}}J_{\text{O}}} & 0 & 0 & if_{J_{\text{O}}e} & f_{J_{\text{Al}}J_{\text{O}}} & f_{J_{\text{O}}J_{\text{O}}} & 0 \\ 0 & 0 & if_{J_{\text{Al}}e} & if_{J_{\text{O}}e} & 0 & 0 & 0 & f_{\dot{e}\dot{e}} \end{pmatrix}, \quad (10)$$

and a matrix of Laplace-transformed time correlation functions at  $z=0$ ,

$$\tilde{\mathbf{F}}(k, z=0) = \begin{pmatrix} \tau_{n_{\text{Al}}n_{\text{Al}}}f_{n_{\text{Al}}n_{\text{Al}}} & \tau_{n_{\text{Al}}n_{\text{O}}}f_{n_{\text{Al}}n_{\text{O}}} & \frac{im_{\text{Al}}}{k}f_{n_{\text{Al}}n_{\text{Al}}} & \frac{im_{\text{O}}}{k}f_{n_{\text{Al}}n_{\text{O}}} & \tau_{n_{\text{Al}}e}f_{n_{\text{Al}}e} & 0 & 0 & f_{n_{\text{Al}}e} \\ \tau_{n_{\text{Al}}n_{\text{O}}}f_{n_{\text{Al}}n_{\text{O}}} & \tau_{n_{\text{O}}n_{\text{O}}}f_{n_{\text{O}}n_{\text{O}}} & \frac{im_{\text{Al}}}{k}f_{n_{\text{Al}}n_{\text{O}}} & \frac{im_{\text{O}}}{k}f_{n_{\text{O}}n_{\text{O}}} & \tau_{n_{\text{O}}e}f_{n_{\text{O}}e} & 0 & 0 & f_{n_{\text{O}}e} \\ \frac{im_{\text{Al}}}{k}f_{n_{\text{Al}}n_{\text{Al}}} & \frac{im_{\text{Al}}}{k}f_{n_{\text{Al}}n_{\text{O}}} & 0 & 0 & \frac{im_{\text{Al}}}{k}f_{n_{\text{Al}}e} & f_{J_{\text{Al}}J_{\text{Al}}} & 0 & 0 \\ \frac{im_{\text{O}}}{k}f_{n_{\text{Al}}n_{\text{O}}} & \frac{im_{\text{O}}}{k}f_{n_{\text{O}}n_{\text{O}}} & 0 & 0 & \frac{im_{\text{O}}}{k}f_{n_{\text{O}}e} & 0 & f_{J_{\text{O}}J_{\text{O}}} & 0 \\ \tau_{n_{\text{Al}}e}f_{n_{\text{Al}}e} & \tau_{n_{\text{O}}e}f_{n_{\text{O}}e} & \frac{im_{\text{Al}}}{k}f_{n_{\text{Al}}e} & \frac{im_{\text{O}}}{k}f_{n_{\text{O}}e} & \tau_{ee}f_{ee} & 0 & 0 & f_{ee} \\ 0 & 0 & -f_{J_{\text{Al}}J_{\text{Al}}} & 0 & 0 & 0 & 0 & if_{J_{\text{Al}}e} \\ 0 & 0 & 0 & -f_{J_{\text{O}}J_{\text{O}}} & 0 & 0 & 0 & if_{J_{\text{O}}e} \\ -f_{n_{\text{Al}}e} & -f_{n_{\text{O}}e} & 0 & 0 & -f_{ee} & if_{J_{\text{Al}}e} & if_{J_{\text{O}}e} & 0 \end{pmatrix}, \quad (11)$$

where the indices in matrix elements correspond to dynamic variables from the set (2). Since among the variables of the set (2) are first-time derivatives of hydrodynamic ones, one can make use of the rules of taking time derivatives and integrals of time correlation functions [44], which allows one to express the matrix elements of Eqs. (10) and (11) via a smaller number of static averages. For this purpose we used the notations  $f_{ij}$ , which correspond to the absolute value of the corresponding static averages, which allowed us to show explicitly for readers which matrix elements are purely imaginary and positive/negative real numbers. The correlation times in Eq. (11) are defined as

$$\tau_{ij}(k) = \frac{1}{F_{ij}(k, t=0)} \int_0^\infty F_{ij}(k, t) dt \quad i, j = n_{\text{Al}}, n_{\text{O}}, e. \quad (12)$$

The eigenvalues of the generalized hydrodynamic matrix  $\mathbf{T}(k)$  and the corresponding eigenvectors allow one to calculate time correlation functions between any two dynamic variables from the set (2),  $i, j = \mathbf{A}^{(8)}(k, t)$ , within the proposed thermoviscoelastic dynamic model and to compare them to the AIMD-derived time correlation functions. The GCM theoretical time correlation functions exactly satisfy a number of exact sum rules, up to the fourth frequency moments of partial dynamic structure factors.

While all the matrix elements corresponding to the six-variable viscoelastic dynamic model can easily be obtained from classical and *ab initio* simulations, the sampling of energy (heat) density fluctuations and corresponding energy (heat)-current density is extremely sophisticated in AIMD (as it was discussed in Ref. [28]), which makes analysis within the eight-variable thermoviscoelastic dynamic model problematic. Therefore, in Ref. [28] it was suggested to treat the nine matrix elements involving quantities with energy (heat) density and energy (heat)-current density as fitting parameters and estimate these fitting parameters from the best correspondence between AIMD-derived three partial density-density and three partial current-current time correlation functions and their GCM theoretical representations. An algorithm of minimization with Powell's conjugate direction method [45] was applied in the fitting scheme. In Ref. [28], using molten NaCl as a case study, very good agreement was obtained between the AIMD simulations and the eight-variable GCM thermoviscoelastic theory. Here, this methodology is applied to much more sophisticated dynamics of molten  $\text{Al}_2\text{O}_3$  and analysis of time correlations in it. All the static and dynamic correlation functions, calculated from AIMD simulations, are estimated in a wide range of wave numbers with the smallest accessible one being  $k_{\min} = 0.4146 \text{ \AA}^{-1}$  and averaged over all possible directions of corresponding wave vectors.

### III. RESULTS AND DISCUSSION

The static atomic structure of binary liquids is usually represented by partial pair distribution functions  $g_{ij}(r)$  and partial structure factors  $S_{ij}(k)$ . In Fig. 1 the partial functions  $g_{ij}(r)$ ,  $i, j = \text{Al}$  and  $\text{O}$ , obtained from AIMD trajectories are shown. As it is typical with long-range Coulomb interaction between particles, the effect of screening of the long-range

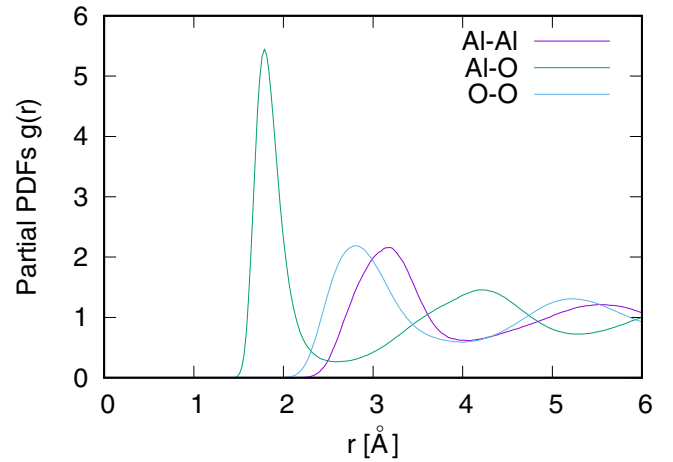


FIG. 1. Partial pair distribution functions for liquid  $\text{Al}_2\text{O}_3$ , obtained from *ab initio* simulations.

attraction results in the first coordination shell (centered at  $\sim 1.85 \text{ \AA}$ ), which is composed of particles with opposite effective charge. The second coordination shell is composed mainly of particles with the same effective charge sign, and as it follows from Fig. 1, Al and O ions have different effective sizes. Partial static structure factors for  $\text{Al}_2\text{O}_3$ , estimated directly from AIMD as  $S_{ij}(k) = \langle n_i(-k)n_j(k) \rangle$  with  $n_i(k, t)$ ,  $i = \text{Al}, \text{O}$ , being the dynamic variables of partial particle density from the set (2) and  $\langle \dots \rangle$ , the ensemble average, are shown in Fig. 2(a). For comparison, Fig. 2(b) shows the  $k$  dependence of Bhatia-Thornton structure factors,  $S_{NN}(k)$  and  $S_{CC}(k)$ , which show correlations in total number ( $N$ ) and concentration ( $C$ ) fluctuations in the binary melt [46,47]. Note that, while the partial structure factors  $S_{\text{AlAl}}(k)$  and  $S_{\text{OO}}(k)$  show qualitatively similar behavior vs  $k$  with peak locations at  $2.5$  and  $2.8 \text{ \AA}^{-1}$ , respectively, the Bhatia-Thornton structure factors show well-pronounced chemical ordering [high first maximum of  $S_{CC}(k)$  at  $\sim 2.6 \text{ \AA}^{-1}$ ] and an absence of a well-pronounced first maximum of  $S_{NN}(k)$ , which is the consequence of specific structural features of molten  $\text{Al}_2\text{O}_3$  observed in partial pair distribution functions in Fig. 1.

Velocity autocorrelation functions (VACFs) are important single-particle time correlation functions, which with Fourier spectra allow estimation of the self-diffusion coefficients, as well as information about the high-frequency vibrational density of states. Figure 3 shows VACFs for Al and O and their Fourier spectra. Since aluminum ions are almost by 70% heavier than the oxygen ones, their VACF do not show well-defined oscillations, although both VACFs in Fig. 3(a) show the ‘‘cage effect,’’ a back-scattering on nearest neighbors, which is evidenced by negative region of the VACFs. The diffusion coefficients estimated from the Kubo-Green integration of VACFs are  $0.175 \pm 0.02$  and  $0.192 \pm 0.02 \text{ \AA}^2/\text{ps}$  for Al and O, respectively. The diffusion of atoms is reflected in nonzero values of VACF Fourier spectra at  $\omega = 0$ . The VACF Fourier spectra usually show peaks at the flat regions in the dispersion of collective excitations. It is worth noting for further analysis of dispersion law that the well-pronounced peaks of VACF Fourier spectra [Fig. 3(b)] are at  $\sim 45 \text{ ps}^{-1}$  for Al and at  $\sim 50 \text{ ps}^{-1}$  for O, while a smeared shoulder is

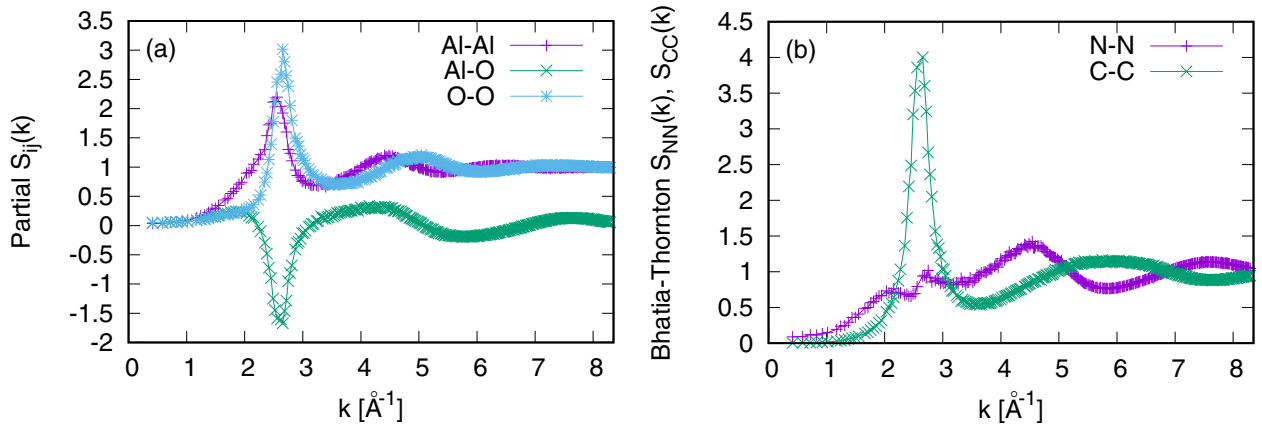


FIG. 2. (a) Partial Ashcroft-Langreth structure factors and (b) Bhatia-Thornton structure factors  $S_{NN}(k) = \langle n_i(-k)n_i(k) \rangle$  and  $S_{CC}(k) = \langle n_c(-k)n_c(k) \rangle$  for liquid  $\text{Al}_2\text{O}_3$ , obtained from *ab initio* simulations.

observed in the VACF Fourier spectrum of oxygen in the region  $\sim 130\text{--}160 \text{ ps}^{-1}$ . Collective dynamics of binary (and in general of many-component) liquids contain nonhydrodynamic excitations caused by mass-concentration fluctuations and which have an analogy with damped optic phonons in many-component solids. The theory of longitudinal (L) [48] and transverse (T) [49] optic modes in binary liquids based on separate treatment of mass-concentration fluctuations results in damping of optic modes due to mutual diffusivity of species and a tendency to demixing. So far, the general theory which accounts for coupling of optic and acoustic modes in the longitudinal case or with fluctuations of total mass current in the transverse case was not derived, because it requires analytical solution of (at least) six-variable longitudinal and four-variable transverse eigenvalue problems. For ionic liquids there are specific features in the behavior of optic modes [20], which come from the local electroneutrality condition which excludes the demixing because the long-wavelength charge-charge static structure factor (an analogy of the Bhatia-Thornton concentration-concentration static structure factor) asymptotically tends to zero. The existence of opticlike excitations in the studied molten  $\text{Al}_2\text{O}_3$  can be seen from the behavior of autocorrelation functions of mass-concentration current  $F_{J_x, J_x}^{L,T}(k, t)$  shown in Fig. 4 at the smallest wave number

available in actual simulations. The dynamic variable of the mass-concentration current  $J_x(k, t)$  is orthogonal to the total mass-current  $J_t(k, t)$  as it was shown in Ref. [49]. One can see in Fig. 4 that the autocorrelation functions of total  $F_{J_t, J_t}^{L/T}(k, t)$  and mass-concentration  $F_{J_x, J_x}^{L/T}(k, t)$  currents indeed correspond to collective processes on different timescales, showing essentially different frequencies of damped oscillations in their time dependence: the long-wavelength functions  $F_{J_x, J_x}^{L/T}(k, t)$  reflect propagation of acoustic excitations in L dynamics and shear waves in T dynamics, while L and T optic modes contribute to  $F_{J_x, J_x}^{L/T}(k, t)$ . This property of  $F_{J_x, J_x}^{L/T}(k, t)$  and  $F_{J_t, J_t}^{L/T}(k, t)$  time correlation functions is used for numerical estimates of the dispersion of L and T collective excitations *via* numerical time Fourier transform.

It is a great challenge for a theory to recover the AIMD-derived time correlation functions. Moreover, if the theory is able to represent the time correlation functions *via* dynamic eigenmodes of the liquid system, then recovering AIMD-derived time correlation functions simultaneously results in dispersion and damping of propagating modes. Two dynamic models are applied, the viscoelastic one for binary liquids with the set of six dynamic variables (6) and the thermo-viscoelastic model of eight dynamic variables (2). In Fig. 5 one can see how the parameter-free viscoelastic six-variable

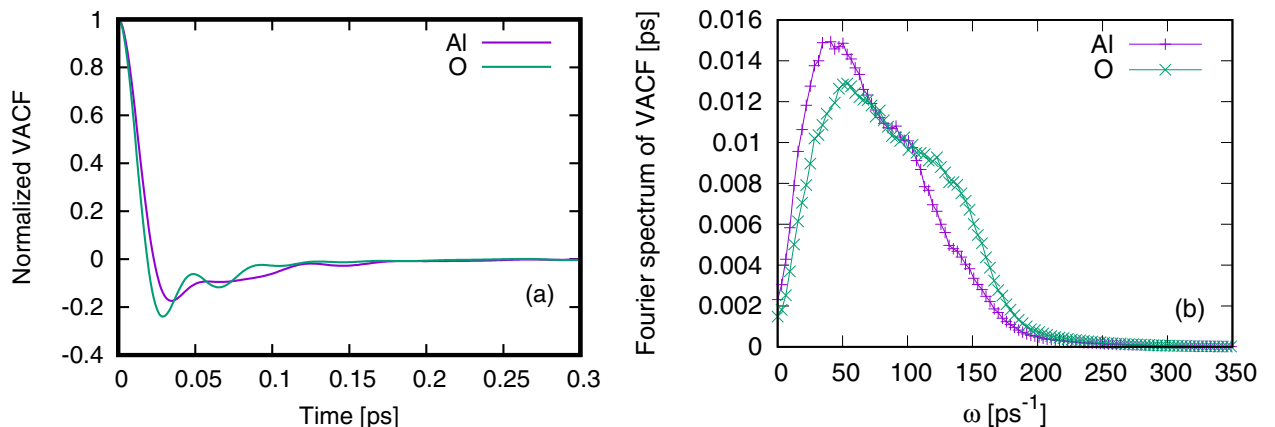


FIG. 3. (a) Normalized velocity autocorrelations functions for Al and O ions and (b) their Fourier spectra.

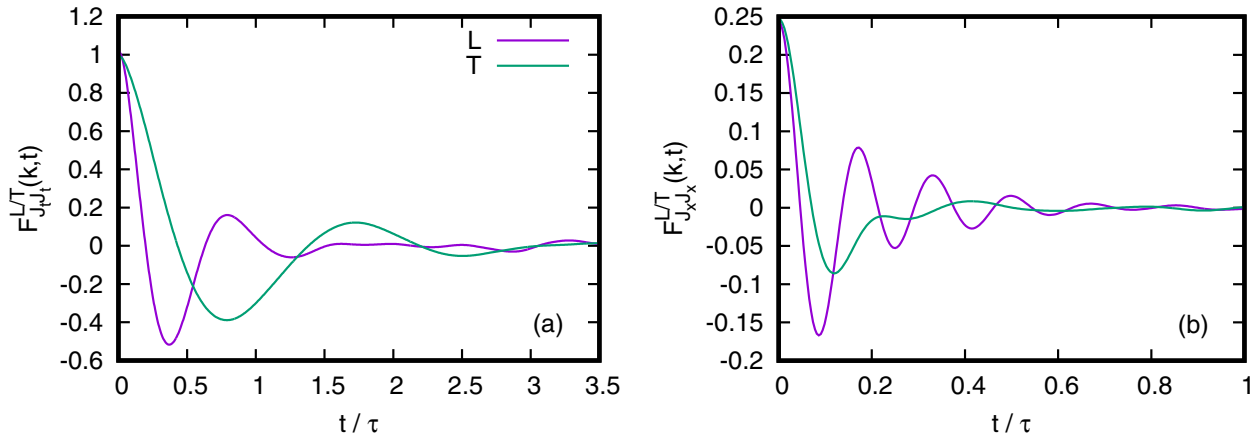


FIG. 4. Autocorrelation functions of longitudinal (L) and transverse (T) total mass-current ( $J_t$ ) and mass-concentration current ( $J_x$ ) at  $k = 0.4146 \text{ \AA}^{-1}$ . The timescale  $\tau$  is 0.243 813 ps.

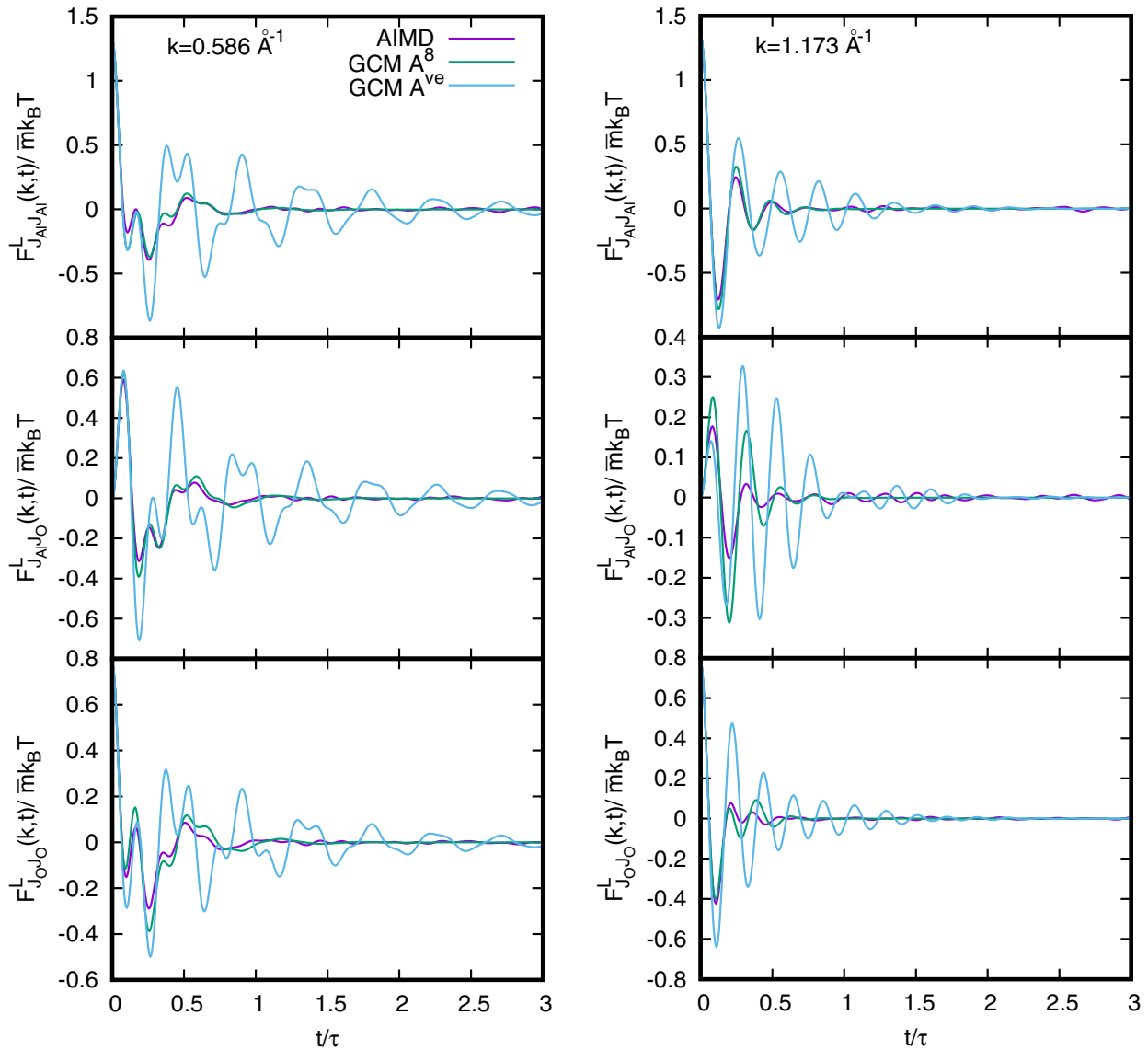


FIG. 5. Partial longitudinal current-current time correlation functions, obtained from *ab initio* simulations (solid lines), and their theoretical GCM replicas within the six-variable viscoelastic model  $A^{(ve)}$  (short-dashed line) and the eight-variable GCM scheme  $A^{(8)}$  (long-dashed line) at two wave numbers  $k$ . The timescale  $\tau$  is 0.243 813 ps.

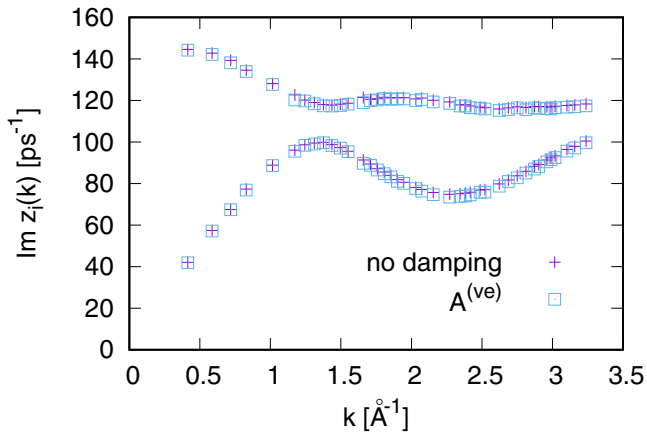


FIG. 6. Dispersion of “bare” (nondamped) longitudinal collective modes (plus symbols) and of propagating eigenmodes obtained within the six-variable model  $A^{(ve)}$  (open boxes).

model is unable to recover correctly the time dependence of partial current-current time correlation functions, while the thermoviscoelastic dynamic model with several parameters, corresponding to coupling with thermal modes, allows one to recover the AIMD-derived time correlation functions in a wide range of wave numbers. Note that both theoretical models,  $A^{(ve)}$  and  $A^{(8)}$ , provide the same precision from the point of view of accounting for frequency and time moments. However, the eight-variable model (2) allows two additional nonhydrodynamic modes. In Fig. 5 each of the GCM theoretical partial current-current functions (either in model  $A^{(ve)}$  or in model  $A^{(8)}$ ) satisfies six sum rules: three for zero-, first-, and second-time derivatives at  $t = 0$  (short-time behavior) and three for the zero-, first-, and second-time moments of  $F_{j,j}^L(k, t)$ . However, two additional nonhydrodynamic eigenmodes within the thermoviscoelastic model allow essential improvement in recovering the AIMD-derived partial current-current functions (as shown in Fig. 5). The issue of unsatisfactory recovering of AIMD-derived current-current time correlation functions by the six-variable viscoelastic model (6) in Fig. 5 becomes clear after comparison of the

dispersion of two branches of propagating eigenmodes, obtained within the viscoelastic model (6), with the frequencies of “bare” (nondamped) collective modes, whose analytical expressions were reported in Ref. [24] (see Fig. 6). Indeed, the frequencies of propagating eigenmodes of the viscoelastic model are just a bit lower than the frequencies of the “bare” modes, showing that some damping mechanism was not taken into account within the simple viscoelastic model, because usually the frequencies of collective modes are renormalized from their “bare” values as

$$\omega_j(k) = \sqrt{\omega_{j,\text{bare}}^2(k) - \sigma_j^2(k)}. \quad (13)$$

For  $k < 1 \text{ \AA}^{-1}$ , one can easily discriminate between the high-frequency opticlike and low-frequency acoustic branches, although the frequencies of the acoustic branch in Fig. 6 are higher than the frequencies of the experimental long-wavelength dispersion of acoustic modes from IXS experiments [7]. It is clear that in the long-wavelength region the acoustic branch is missing additional damping due to coupling with thermal fluctuations [the viscoelastic model (6) does not have thermal processes among the dynamic variables], which make the leading contribution to the central peak of dynamic structure factor (and to exponential decay of all partial density-density time correlation functions) according to the hydrodynamics of molten salts [44]. Figure 5 shows evidence that the thermoviscoelastic model, in contrast to the six-variable model, is able to recover the behavior of AIMD-derived time correlation functions. The dispersion and damping of propagating modes obtained within the eight-variable thermoviscoelastic model  $A^{(8)}$  and contributing to the behavior of partial current-current time correlation functions are shown in Fig. 7. In almost the whole  $k$ -range three pairs of complex-conjugated eigenvalues  $z_j(k) = \sigma_j(k) \pm i\omega_j(k)$ ,  $j = 1$  and 3, of dynamic modes were obtained, where  $\omega_j(k)$  and  $\sigma_j(k)$  are dispersion and damping of the  $j$ th propagating mode. In Fig. 7 one can see that for  $k < 1 \text{ \AA}^{-1}$  it is easy to distinguish three branches of propagating excitations, while for larger wave numbers the coupling between branches leads to essential mixing of contributions from different types of microscopic fluctuations reflected in dynamic variables of the

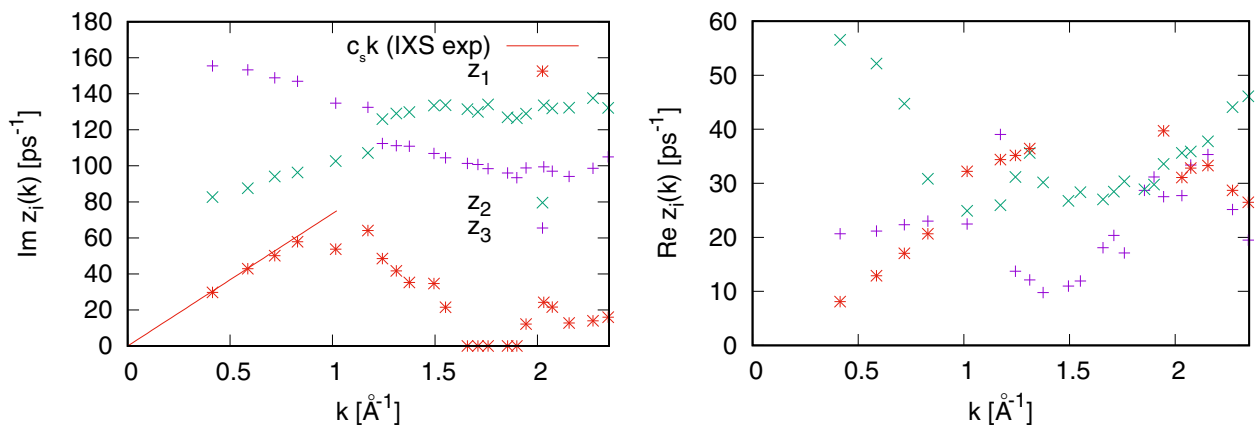


FIG. 7. Imaginary (frequency) and real (damping) parts of propagating eigenmodes obtained by theoretical GCM analysis of AIMD-derived time correlation functions within the thermoviscoelastic model  $A^{(8)}$ . The straight line in the left frame corresponds to the linear hydrodynamic dispersion with the speed of sound taken from Ref. [7].

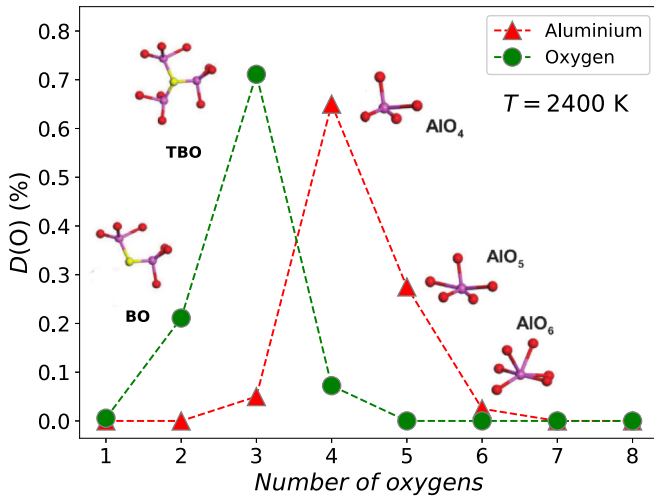


FIG. 8. Distribution of the number of oxygen atoms around aluminium (triangles) and oxygen (circles) from AIMD simulation at  $T = 2400$  K. Insets show typical local structural units present with significant proportions around O atoms (shown in yellow color) such as bonded oxygen (BO) and triply bonded oxygen (TBO), also called triclusters, as well as around Al atoms, such as  $\text{AlO}_4$ ,  $\text{AlO}_5$ , and  $\text{AlO}_6$ . Al and O atoms are drawn in magenta and red, respectively.

set  $A^{(8)}$  (2) and it is difficult to estimate the unique origin of each dynamic mode. In the low- $k$  region it is easy to identify at least two branches of propagating modes. The branch  $z_1(k)$  corresponds to acoustic excitations, which propagate with an apparent speed of sound very close to the linear dispersion law estimated from IXS experiments [7]. From the propagating eigenmode at the lowest  $k$  value we estimated the speed of sound in liquid alumina at  $T = 2400$  K to be  $7180$  m/s, which agrees with the experimental data [7]:  $7350 \pm 40$  m/s at  $2323$  K and considering that with temperature the IXS experiments estimated a drop of the speed of sound to  $6530 \pm 70$  m/s at  $3073$  K. Another branch  $z_3(k)$  corresponds to the longitudinal optic (LO) excitations. Being nonhydrodynamic excitations (which are not caused by fluctuations of conserved quantities), the damping of the LO branch  $z_3(k)$  tends in the long-wavelength limit to a constant value of  $\sim 20$  ps $^{-1}$ , which makes it evident that the nonhydrodynamic modes do not contribute to the dynamics on macroscopic scales, in comparison with the hydrodynamic asymptote of damping of acoustic excitations  $\sim k^2$ , i.e., extremely long lifetimes of the long-wavelength acoustic modes. The branch of propagating modes  $z_2(k)$  has much stronger damping in the long-wavelength region, which rapidly decreases with increasing  $k$ . The smooth dependence of the dispersion and damping of the mode  $z_2(k)$  for  $k < 1$  Å $^{-1}$  implies its relation to a well-defined collective process, although in that frequency range only transverse optic (TO) modes exist. It is very unusual in the dynamics of binary liquids to observe in longitudinal dynamics a possible contribution from transverse modes, however, for melts with long-range Coulomb interaction the coupling between longitudinal and transverse modes can exist, as it was shown for the case of water [50].

Besides, in the region  $k > 1$  Å $^{-1}$  it is extremely difficult to assign the propagating modes to some specific collective

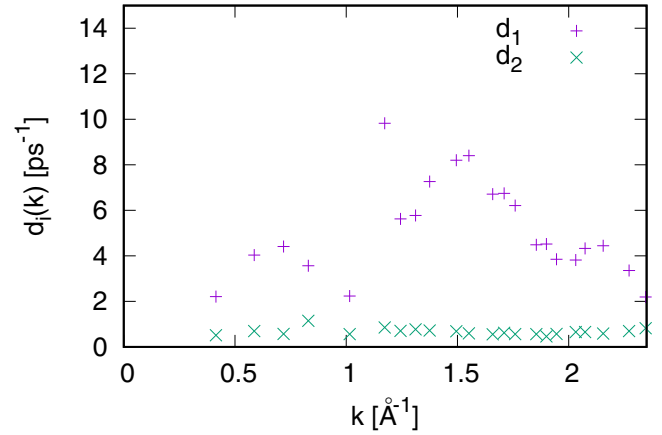


FIG. 9. Purely relaxing (real) eigenmodes obtained by theoretical GCM analysis of AIMD-derived time correlation functions within the thermoviscoelastic model  $A^{(8)}$ .

processes because of the coupling between them and because of contributions to dynamics of significantly diverse local short-time living structural units. As a matter of fact, Fig. 8 shows the distribution of the number of oxygen around aluminium and oxygen, showing a variety of local structural units such as  $\text{AlO}_3$ ,  $\text{AlO}_4$ ,  $\text{AlO}_5$ , and  $\text{AlO}_6$  as well as oxygen bonding linking them. In many oxides, the usual networks forming structure are characterized by bonded oxygens (BO) linking tetrahedral structural units ( $\text{MO}_4$ , with  $M$  being the metal center), as, for instance, in the prototypical case of  $\text{SiO}_2$  or  $\text{GeO}_2$ . The structure of  $\text{Al}_2\text{O}_3$  is more complex with the appearance, among others, of fivefold coordinated Al,  $\text{AlO}_5$ , in significant proportions, and triply bonded oxygen (TBO), both being known to play a role in the shear viscosity [6] and hence the collective dynamics.

Along with three branches of propagating solutions  $z_j(k) = \sigma_j(k) \pm i\omega_j(k)$ , the eight-variable thermoviscoelastic dynamic model results in two purely real eigenmodes  $d_j(k) \equiv \text{Re}[z_j(k)]$ , where the real eigenmodes are denoted as  $d_j(k)$  in order to distinguish them among eight GCM eigenmodes  $z_j(k)$  of the thermoviscoelastic model. Figure 9 displays the  $k$  dependence of the two real eigenmodes. In the region  $k$   $1.55$ – $1.85$  Å $^{-1}$ , two additional purely real eigenmodes emerge instead of the complex-conjugated pair  $z_1(k)$ ; however, their eigenvalues  $d_{3,4}(k) \gg d_1(k), d_2(k)$ ; therefore, they are not shown in Fig. 9. For liquids with long-range Coulomb interactions the very specific behavior of long-wavelength relaxation processes is the absence of the  $\sim k^2$  asymptote for the relaxing mode associated with the electric conductivity, while in simple liquid mixtures the direct analogy for that mode is the relaxation connected with mutual diffusivity tending in the long-wavelength limit as  $Dk^2$ , where  $D$  is a combination of mutual and thermal diffusivities [51]. For molten  $\text{Al}_2\text{O}_3$ , the purely relaxing mode  $d_2(k)$  in Fig. 9 tends to a nonzero constant value in the long-wavelength limit as it should be for molten salts, while another purely relaxing mode  $d_1(k)$  is connected with thermal diffusivity and should have the asymptotic behavior  $D_T k^2$ , with  $D_T$  being the thermal diffusivity (diffusivity of local temperature).

As a next step, the GCM propagating eigenmodes are compared to the numerical estimates of excitation frequencies



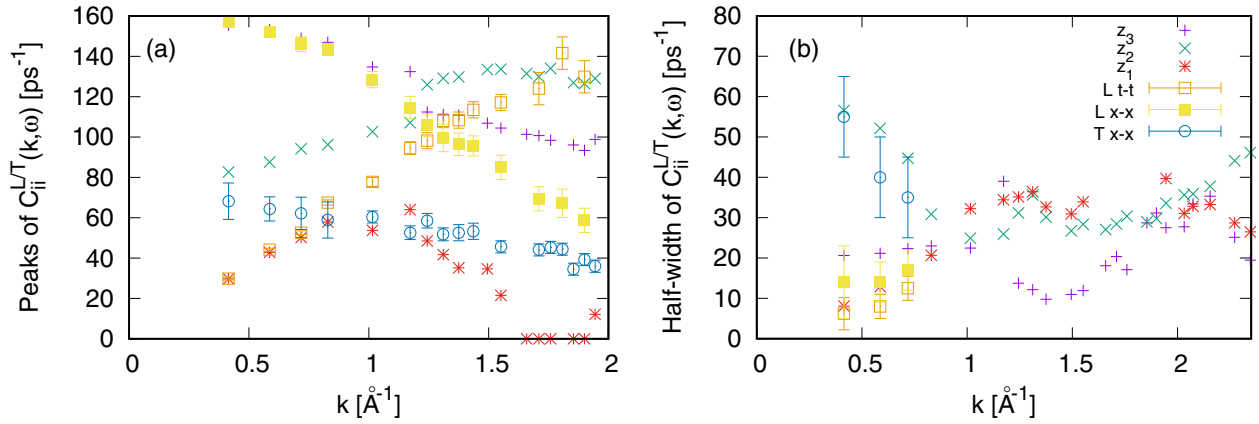


FIG. 10. Numerical estimates for dispersions and damping of propagating collective modes from peak positions and half-width of L and T current-current spectral functions  $C_{ii}^{L/T}(k, \omega)$ ,  $i = t$  and  $x$ , in comparison with the imaginary (dispersion) and real (damping) parts of complex eigenmodes.

and damping from the current spectral function  $C_{ii}^{L/T}(k, \omega)$ ,  $i = t$  and  $x$ , where the indices  $t$  and  $x$  correspond to the total mass current and mass-concentration current, respectively. In Fig. 10 the frequencies and damping of the three branches of collective eigenmodes are compared with the peak position and half-width at half-height (HWHH) of longitudinal  $C_{ii}^L(k, \omega)$ ,  $i = t$  and  $x$  (open and solid boxes with error bars), and transverse  $C_{xx}^T(k, \omega)$  (open circles with error bars). One has to keep in mind that separate treatment of “ $t$ - $t$ ” and “ $x$ - $x$ ” correlations is absolutely justified in the long-wavelength region, where the total current spectral functions contain just a single peak coming from acoustic excitations, while the mass-current spectral function in the case of molten salts and oxide melts reflects the mutual dynamics of charge species, in agreement with the behavior of corresponding time correlation functions shown in Fig. 4. Figure 10 shows that the peak positions of  $C_{ii}^L(k, \omega)$ ,  $i = t$  and  $x$ , and the corresponding HWHH are in perfect agreement with the long-wavelength GCM eigenmodes, longitudinal acoustic branch  $z_1(k)$ , and longitudinal optic branch  $z_3(k)$ . Concerning another propagating branch of GCM eigenmodes,  $z_2(k)$ , it is seen from Fig. 10 that, surprisingly, the long-wavelength frequency and damping of  $z_2(k)$  tend to the same values as those of the transverse optic branch. Recently, the same agreement between the TO dispersion and the behavior of  $z_2(k)$  was observed in the analysis of GCM eigenmodes in molten NaCl [28]. The issue of possible contributions from transverse collective modes to the longitudinal dynamics was discussed after IXS experiments on several liquid metals [52–56], while in computer simulations an effect of L-T coupling was clearly observed for water [50] and the possibility of the L-T coupling effect on simulation-derived current spectral functions was discussed in Refs. [57–59]. However, practically no reports were published before on the possible L-T coupling in ionic melts (and molten salts in particular) and especially on a possible manifestation of TO modes in longitudinal dynamics.

#### IV. CONCLUSION

To conclude, *ab initio* simulations of molten  $\text{Al}_2\text{O}_3$  in combination with the theoretical generalized mode analysis

were performed in order to study collective eigenmodes in the dynamics of this complex oxide melt. The methodology of *ab initio* analysis of collective modes in liquids with long-range interactions consisted of the estimation of the dynamic eigenmodes within the eight-variable treatment of the generalized Langevin equation in matrix  $8 \times 8$  form, which corresponds to the thermoviscoelastic dynamic model. It was shown that the application of the eight-variable thermoviscoelastic model allows one to recover AIMD-derived partial current-current time correlation functions with good precision. This means that eight eigenmodes are able to explain the time dependence of longitudinal partial current correlations. For comparison, the standard six-variable dynamic model was not able to recover the same partial current-current correlations.

Among eight eigenmodes, for most  $k$  points we obtained three pairs of complex-conjugated eigenvalues and two purely real ones. We identified the low-frequency branch as the longitudinal acoustic branch with practically linear dispersion in the long-wavelength region, the slope of which corresponds to the sound propagation speed in good agreement with IXS experiments [7]. The high-frequency branch corresponds to the longitudinal optic branch with the frequency decreasing and the damping increasing with  $k$  in the long-wavelength region, respectively. Surprisingly, the nondamped (“bare”) optic eigenmodes and those obtained within the six-variable viscoelastic dynamic model tend to a frequency of  $\omega_{\text{opt}}(k = 0) \sim 148 \text{ ps}^{-1}$  (Fig. 6), while the numerical estimates of the dispersion for the LO branch from peak positions of  $C_{xx}^L(k, \omega)$  indicate the value  $\omega_{\text{opt}}(k = 0) \sim 160 \text{ ps}^{-1}$  (Fig. 10); this implies the absence of additional coupling to propagating processes in the models with solely two LA and LO branches. The eight-variable dynamic model allowed us to obtain another branch of nonhydrodynamic excitations,  $z_2(k)$ , and essentially improved the recovering of the partial current-current time correlation functions (and consequently their spectral functions).

The origin of the additional propagating eigenmode  $z_2(k)$ , which allows essential correction of the time correlation functions and of the long-wavelength frequency of LO modes, remains unclear. Surprisingly, the long-wavelength limit of the frequency of  $z_2(k)$  tends to the frequency of

long-wavelength TO excitations, and so do also their dampings, where both frequencies and damping of TO modes were estimated from peak positions and HWHH of  $C_{xx}^T(k, \omega)$ . However, at the moment we cannot suggest a mechanism of possible LO-TO coupling in molten ionic liquid, while the direct local coupling (with the same  $k$ ) is obviously zero for fluctuating L and T mass-concentration currents. However, our analysis of dynamic eigenmodes makes it evident that an additional propagating mode [in our case  $z_2(k)$ ] essentially improves the recovering of current-current time correlation functions and of the frequencies of long-wavelength LO modes.

### ACKNOWLEDGMENTS

The calculations have been performed using the *ab initio* total-energy and molecular dynamics program VASP (Vienna *ab initio* simulation program) developed at the

Institute für Materialphysik of the Universität Wien. M.K. and T.B. were supported by the National Research Foundation of Ukraine under Grant No. 2020.02/0115. N.J. acknowledges the CINES, IDRIS, and TGCC under Project No. INP2227/92914/gen5054 as well as GRICAD (Grenoble Alpes Recherche–Infrastructure de Calcul Intensif et de Données) for computing resources. This work has been partially supported by MIAI@Grenoble Alpes (Grant No. ANR-19-P3IA-0003) and international SOLIMAT Project No. ANR-22-CE92-0079-01. We appreciate discussions within the French collaborative network for artificial intelligence in materials science GDR CNRS 2123 (IAMAT). J.-F.W. also acknowledges PMMS (Pôle Messin de Modélisation et de Simulation), for computational resources. This work was performed within the framework of the Centre of Excellence of Multifunctional Architected Materials “CEMAM” under Grant No. ANR-10-LABX-44-01 funded by the “Investments for the Future” Program.

- 
- [1] M. Niedźwiedź, W. Skoneczny, M. Bara, and G. Dercz, *Coatings* **11**, 1294 (2021).
- [2] K. A. M. Attia, A. M. Abdel-Raoof, A. Serag, S. M. Eld, and A. E. Abbas, *RSC Adv.* **12**, 17536 (2022).
- [3] S. A. Mahmoud, M. E. Elsisy, and A. F. Mansour, *Sci. Rep.* **12**, 17009 (2022).
- [4] D. R. Crapper, S. S. Krishnan, and A. J. Dalton, *Science* **180**, 511 (1973).
- [5] M. Kawahara and M. Kato-Negishi, *Int. J. Alzheimer’s Dis.* **2011**, 276393 (2011).
- [6] N. Jakse, M. Bouhadja, J. Kozaily, J. W. E. Drewitt, L. Hennet, D. R. Neuville, H. E. Fischer, V. Cristiglio, and A. Pasturel, *Appl. Phys. Lett.* **101**, 201903 (2012).
- [7] H. Sinn, B. Glorieux, L. Hennet, A. Alatas, M. Hu, E. E. Alp, F. J. Bermejo, D. L. Price, and M.-L. Saboungi, *Science* **299**, 2047 (2003).
- [8] S. J. Schneider, *Pure Appl. Chem.* **21**, 115 (1970).
- [9] L. B. Skinner, A. C. Barnes, Ph. S. Salmon, L. Hennet, H. E. Fischer, C. J. Benmore, S. Kohara, J. K. Richard Weber, A. Bytchkov, M. C. Wilding, J. B. Parise, T. O. Farmer, I. Pozdnyakova, S. K. Tumber, and K. Ohara, *Phys. Rev. B* **87**, 024201 (2013).
- [10] M. Hemmati, M. Wilson, and P. A. Madden, *J. Phys. Chem. B* **103**, 4023 (1999).
- [11] G. Gutierrez, A. B. Belonoshko, R. Ahuja, and B. Johansson, *Phys. Rev. E* **61**, 2723 (2000).
- [12] S. Jahn, P. A. Madden, and M. Wilson, *Phys. Rev. B* **74**, 024112 (2006).
- [13] S. Jahn and P. A. Madden, *J. Non-Cryst. Solids* **353**, 3500 (2007).
- [14] S. Jahn and P. A. Madden, *Condens. Matter Phys.* **11**, 169 (2008).
- [15] M. Bouhadja and N. Jakse, *J. Phys.: Condens. Matter* **32**, 104002 (2020).
- [16] N. Jakse, C. M. S. Alvares, and A. Pisch, *J. Phys.: Condens. Matter* **33**, 285401 (2021).
- [17] J. Sun, A. Ruzsinszky, and J. P. Perdew, *Phys. Rev. Lett.* **115**, 036402 (2015).
- [18] I. M. Mryglod, I. P. Omelyan, and M. V. Tokarchuk, *Mol. Phys.* **84**, 235 (1995).
- [19] T. Bryk, I. Mryglod, and G. Kahl, *Phys. Rev. E* **56**, 2903 (1997).
- [20] T. Bryk and I. Mryglod, *J. Phys.: Condens. Matter* **16**, L463 (2004).
- [21] T. Bryk and I. Mryglod, *Phys. Rev. B* **71**, 132202 (2005).
- [22] F. Demmel, S. Hosokawa, M. Lorenzen, and W.-C. Pilgrim, *Phys. Rev. B* **69**, 012203 (2004).
- [23] F. Demmel, S. Hosokawa, W.-C. Pilgrim, and S. Tsutsui, *Nucl. Instrum. Methods Phys. Res., Sect. B* **238**, 98 (2005).
- [24] T. Bryk and I. Mryglod, *Chem. Phys. Lett.* **466**, 56 (2008).
- [25] T. Bryk and I. Mryglod, *Phys. Rev. B* **79**, 184206 (2009).
- [26] S. Hosokawa, M. Inui, T. Bryk, I. Mryglod, W.-C. Pilgrim, Y. Kajihara, K. Matsuda, Y. Ohmasa, and S. Tsutsui, *Condens. Matter Phys.* **22**, 43602 (2019).
- [27] F. Demmel, S. Hosokawa, and W.-C. Pilgrim, *J. Phys.: Condens. Matter* **33**, 375103 (2021).
- [28] T. Bryk, M. Kopcha, and G. Ruocco, *J. Mol. Liq.* **387**, 122622 (2023).
- [29] P. Hohenberg and W. Kohn, *Phys. Rev.* **136**, B864 (1964).
- [30] W. Kohn and L. J. Sham, *Phys. Rev.* **140**, A1133 (1965).
- [31] G. Kresse and J. Hafner, *Phys. Rev. B* **48**, 13115 (1993).
- [32] G. Kresse and J. Hafner, *Phys. Rev. B* **49**, 14251 (1994).
- [33] G. Kresse and J. Furthmüller, *Comput. Mater. Sci.* **6**, 15 (1996).
- [34] G. Kresse and D. Joubert, *Phys. Rev. B* **59**, 1758 (1999).
- [35] C. M. S. Alvares, G. Deffrennes, A. Pisch, and N. Jakse, *J. Chem. Phys.* **152**, 084503 (2020).
- [36] G. Deffrennes, N. Jakse, C. M. S. Alvares, I. Nuta, A. Pasturel, A. Khvan, and A. Pisch, *CALPHAD* **69**, 101764 (2020).
- [37] M. P. Allen and D. J. Tildesley, *Computer Simulation of Liquids* (Oxford University, Oxford, 1989).
- [38] B. Smit and D. Frenkel, *Understanding Molecular Simulations*, 2nd ed. (Academic, San Diego, 2002).
- [39] J. E. Basconi and M. R. Shirts, *J. Chem. Theory Comput.* **9**, 2887 (2013).
- [40] M. Lucht, M. Lerche, H. C. Wille, Y. V. Shvyd’ko, H. D. Rüter, E. Gerdau, and P. Becker, *J. Appl. Crystallogr.* **36**, 1075 (2003).

- [41] Y. S. Anisimov and B. S. Mitin, *Izv. Akad. Nauk SSSR. Neorg. Mater.* **13**, 1442 (1977).
- [42] T. Bryk, *Eur. Phys. J. Spec. Top.* **196**, 65 (2011).
- [43] T. Bryk and I. Mryglod, *Phys. Rev. E* **63**, 051202 (2001).
- [44] J.-P. Hansen and I. R. McDonald, *Theory of Simple Liquids*, 3rd ed. (Academic, London, 2006).
- [45] M. J. D. Powell, *Comput. J.* **7**, 155 (1964).
- [46] A. B. Bhatia and D. E. Thornton, *Phys. Rev. B* **2**, 3004 (1970).
- [47] A. B. Bhatia, D. E. Thornton, and N. H. March, *Phys. Chem. Liq.* **4**, 97 (1974).
- [48] T. Bryk and I. Mryglod, *J. Phys.: Condens. Matter* **14**, L445 (2002).
- [49] T. Bryk and I. Mryglod, *J. Phys.: Condens. Matter* **12**, 6063 (2000).
- [50] M. Sampoli, G. Ruocco, and F. Sette, *Phys. Rev. Lett.* **79**, 1678 (1997).
- [51] T. Bryk and J.-F. Wax, *J. Chem. Phys.* **135**, 154510 (2011).
- [52] S. Hosokawa, M. Inui, Y. Kajihara, K. Matsuda, T. Ichitsubo, W.-C. Pilgrim, H. Sinn, L. E. González, D. J. González, S. Tsutsui, and A. Q. R. Baron, *Phys. Rev. Lett.* **102**, 105502 (2009).
- [53] V. M. Giordano and G. Monaco, *Proc. Natl. Acad. Sci. USA* **107**, 21985 (2010).
- [54] V. M. Giordano and G. Monaco, *Phys. Rev. B* **84**, 052201 (2011).
- [55] S. Hosokawa, S. Munejiri, M. Inui, Y. Kajihara, W.-C. Pilgrim, Y. Ohmasa, S. Tsutsui, A. Q. R. Baron, F. Shimojo, and K. Hoshino, *J. Phys.: Condens. Matter* **25**, 112101 (2013).
- [56] S. Hosokawa, M. Inui, Y. Kajihara, S. Tsutsui, and A. Q. R. Baron, *J. Phys.: Condens. Matter* **27**, 194104 (2015).
- [57] T. Bryk, G. Ruocco, T. Scopigno, and A. P. Seitsonen, *J. Chem. Phys.* **143**, 104502 (2015).
- [58] T. Bryk and J.-F. Wax, *J. Chem. Phys.* **144**, 194501 (2016).
- [59] T. Bryk, T. Demchuk, N. Jakse, and J.-F. Wax, *Front. Phys.* **6**, 6 (2018).